Progressive Specification Rather than Intercalation of Segments During Limb Regeneration

Kathleen Roensch *et al.*

Science **342**, 1375 (2013);
DOI: 10.1126/science.1241796

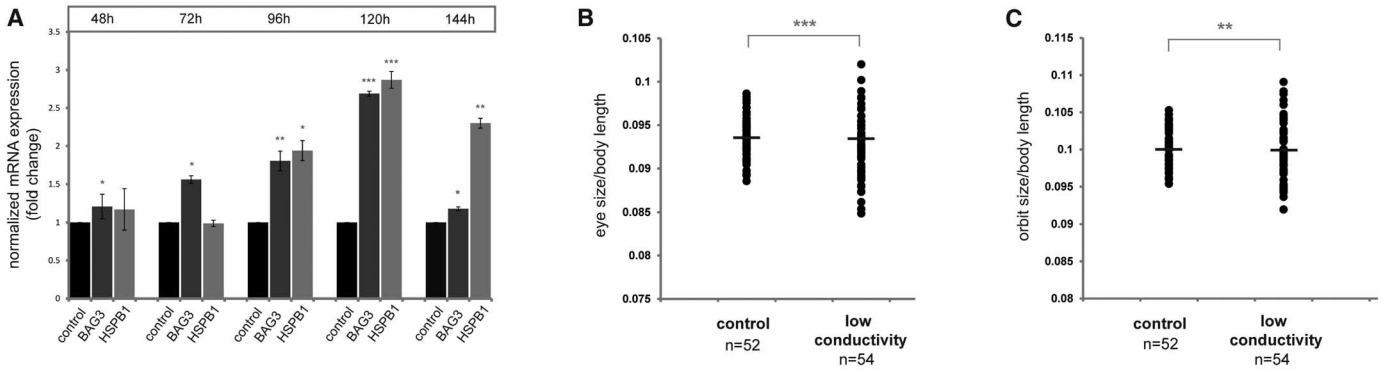

Fig. 4. Low-conductivity conditions in the cave natural habitat have a similar effect to Radicicol treatment on surface populations. (**A**) Quantitative reverse transcription polymerase chain reaction of BAG3 and HSPB1 for surface fish reared under low-conducitivity (230 μS) conditions compared with control conductivity conditions (two-tailed *t* test, $*P < 0.05$; $**P < 0.005$; $***P < 0.0005$). Time scale refers to hours of treatment. (**B** and **C**) Lower-conductivity conditions reveal an increase in variation of (B) orbit size and (C) eye size (eye size SD, +50%; two-sided *F* test, $P = 0.0018$; Bartlett's test, $P = 0.006$; Levene's test, $P = 0.005$; orbit size SD, +58%; two-sided *F* test: $P = 5.9 \times 10^{-4}$; Bartlett's test, $P = 0.001$; Levene's test, $P = 0.01$).

produce a smaller orbit when released from their normal HSP90 interactions. This strongly suggests an involvement of HSP90 in cavefish evolution and provides an actual case in nature for Waddington's classic theory of the role of canalization in evolution. Not all cave-specific traits appear to have relied on HSP90-canalized cryptic variation for their evolution. We examined several other traits and found, for example, that there is no cryptic variation in body size (fig. S6) or in neuromast number (fig. S7) uncovered by HSP90 inhibition in the populations we examined.

It is also reasonable to assume that the change in conductivity is only one factor contributing to the stress response that surface fish might experience after colonizing the caves (such as lower oxygen levels or starvation). However, such environmentally induced stress is likely to have been only transient because the cavefish would have adapted to these new conditions over subsequent generations. Cavefish have higher basal HSP90 levels than those of surface fish (*22*), potentially rendering them more stress-resistant. However, during the transition period when the fish were adapting to the cave conditions, the HSP90-dependent standing variation in eye size we observed in the surface population of *A. mexicanus* would have helped potentiate a rapid response to the cave environment.

Of course, the extreme environment of the cavefish is exceptional in many ways. Yet, environmental challenges are likely to be a driving force for many other adaptations. For example, temperature increases are extremely common in nature, and even simple starvation affects Hsp expression in European Sea Bass (*23*).

References and Notes

1. P. F. Colosimo *et al.*, *Science* **307**, 1928–1933 (2005).
2. F. C. Jones *et al.*, *Nature* **484**, 55–61 (2012).
3. C. H. Waddington, *Nature* **150**, 563–565 (1942).
4. C. H. Waddington, *Evolution* **7**, 118 (1953).
5. S. L. Rutherford, S. Lindquist, *Nature* **396**, 336–342 (1998).
6. C. Queitsch, T. A. Sangster, S. Lindquist, *Nature* **417**, 618–624 (2002).
7. D. F. Jarosz, S. Lindquist, *Science* **330**, 1820–1824 (2010).
8. L. E. Cowen, S. Lindquist, *Science* **309**, 2185–2189 (2005).
9. Y. Xu, M. A. Singer, S. Lindquist, *Proc. Natl. Acad. Sci. U.S.A.* **96**, 109–114 (1999).
10. M. Taipale *et al.*, *Cell* **150**, 987–1001 (2012).
11. D. F. Jarosz, M. Taipale, S. Lindquist, *Annu. Rev. Genet.* **44**, 189–216 (2010).
12. V. Sollars *et al.*, *Nat. Genet.* **33**, 70–74 (2003).
13. D. Mittelman, K. Sykoudis, M. Hersh, Y. Lin, J. H. Wilson, *Cell Stress Chaperones* **15**, 753–759 (2010).
14. G. Chen, W. D. Bradford, C. W. Seidel, R. Li, *Nature* **482**, 246–250 (2012).
15. V. Specchia *et al.*, *Nature* **463**, 662–665 (2010).
16. R. Sawarkar, C. Sievers, R. Paro, *Cell* **149**, 807–818 (2012).
17. M. Protas, M. Conrad, J. B. Gross, C. Tabin, R. Borowsky, *Curr. Biol.* **17**, 452–454 (2007).
18. W. R. Jeffery, *Annu. Rev. Genet.* **43**, 25–47 (2009).
19. T. W. Schulte *et al.*, *Mol. Endocrinol.* **13**, 1435–1448 (1999).
20. P. L. Yeyati, R. M. Bancewicz, J. Maule, V. van Heyningen, *PLoS Genet.* **3**, e43 (2007).
21. C. Y. Choi, K. W. An, *Comp. Biochem. Physiol. B Biochem. Mol. Biol.* **149**, 91–100 (2008).
22. T. A. Hooven, Y. Yamamoto, W. R. Jeffery, *Int. J. Dev. Biol.* **48**, 731–738 (2004).
23. E. Antonopoulou *et al.*, *Comp. Biochem. Physiol. A Mol. Integr. Physiol.* **165**, 79–88 (2013).

Acknowledgments: We thank B. Martineau for animal husbandry and T. Luong for assistance in data acquisition; M. Taipale for HSP90 inhibitor and discussions; H. Boldt and M. Harris for providing zebrafish; L. Espinasa for practical support during the caving expedition; L. Legendre for comparison of environmental parameters; and J. Bibliowicz and Y. Elipot for discussions. N.R. was supported by a Deutsche Forschungsgemeinschaft postdoctoral fellowship (RO 4097/1-1). D.F.J. was supported by a postdoctoral fellowship from Damon Runyon Cancer Research Foundation and a Pathway to Independence Award from the NIH. C.J.T. acknowledges the support of a grant from NIH RO1 HD047360.

Supplementary Materials

www.sciencemag.org/content/342/6164/1372/suppl/DC1
Materials and Methods
Supplementary Text
Figs. S1 to S7
Table S1
References (*24*–*29*)

8 May 2013; accepted 31 October 2013
10.1126/science.1240276

Progressive Specification Rather than Intercalation of Segments During Limb Regeneration

Kathleen Roensch,[1,2]*† Akira Tazaki,[1,2]*† Osvaldo Chara,[3,4] Elly M. Tanaka[1,2]†‡

An amputated salamander limb regenerates the correct number of segments. Models explaining limb regeneration were largely distinct from those for limb development, despite the presence of common patterning molecules. Intercalation has been an important concept to explain salamander limb regeneration, but clear evidence supporting or refuting this model was lacking. In the intercalation model, the first blastema cells acquire fingertip identity, creating a gap in positional identity that triggers regeneration of the intervening region from the stump. We used HOXA protein analysis and transplantation assays to show that axolotl limb blastema cells acquire positional identity in a proximal-to-distal sequence. Therefore, intercalation is not the primary mechanism for segment formation during limb regeneration in this animal. Patterning in development and regeneration uses similar mechanisms.

Numerous models to explain proximodistal metazoan limb patterning during regeneration have been proposed. Cell intercalation has become an important concept based on the results of grafting experiments (*1*–*6*). Cell intercalation is a patterning process whereby experimentally

induced juxtaposition of cells from disparate parts of an organ (for example, upper arm and fingertip) stimulates a proliferative response that restores the missing, intervening portion of the organ. In arthropods, grafting of the distal leg tip onto an amputated upper leg stump stimulated the leg stump and the leg tip cells at the graft junction to proliferate and restore the missing segments until a normal leg was formed (*7*). In salamanders, limb amputation results in the formation of a blastema, a zone of proliferative mesenchymal and epithelial progenitor cells that restores the missing limb elements. When a salamander hand blastema was grafted onto an upper limb stump, intercalation occurred, whereby the upper arm stump regenerated the missing lower arm segment and the grafted hand blastema regenerated the hand (*8*–*10*). The intercalation was unidirectional—the hand blastema cells did not contribute to restoration of the missing lower arm. Unidirectional intercalation reflects a cellular determination state, termed "the rule of distal transformation," in which connective tissue–derived blastema cells can only form limb segments more distal to their original identity (*10*–*13*).

An important question is whether intercalation is an integral part of normal limb regeneration (*1*–*4*). In such models, the first blastema cells acquire a distal (prospective fingertip) identity. This juxtaposion of fingertip progenitors with upper arm cells were proposed to induce the stump cells to intercalate lower arm cells. Tracking of carbon particles or transiently transfected green fluorescent protein (GFP)–expressing limb blastema cells suggested that early- to midstage blastema cells could have distal identity consistent with intercalation (*14*, *15*). However, the data were inconclusive because the labels were not permanently cell-associated.

Expression analysis of posterior *HoxA* family members provided a molecular means to examine the progression of segment identities during limb development and regeneration. During vertebrate limb development, a $HoxA9^{+}HoxA11^{-}HoxA13^{-}$ state reflects progenitor cells for the upper arm, $HoxA9^{+}HoxA11^{+}HoxA13^{-}$ for the lower arm, and $HoxA9^{+}HoxA11^{+}HoxA13^{+}$ for the hand (*16*–*20*). The genes are expressed in a spatial and temporal sequence with *HoxA9* transcripts expressed first throughout the limb bud, followed closely by *HoxA11* more distally and lastly *HoxA13* in the distalmost tip, a phenomenon called temporal and spatial colinearity (*21*–*23*). This expression data coupled with functional studies have favored the conclusion that, during limb development,

[1]Deutsche Forschungsgemeinschaft (DFG)–Center for Regenerative Therapies Dresden, Technische Universität Dresden, Germany. [2]Max Planck Institute of Molecular Cell Biology and Genetics, Dresden, Germany. [3]Center for Information Services and High Performance Computing, Technische Universität Dresden, Germany. [4]Institute of Physics of Liquids and Biological Systems, Consejo Nacional de Investigaciones Científicas y Técnicas (CONICET) and University of La Plata, Argentina.

*These authors contributed equally to this work.
†Present address: DFG–Center for Regenerative Therapies Dresden, Technische Universität Dresden, Germany.
‡Corresponding author. E-mail: elly.tanaka@crt-dresden.de

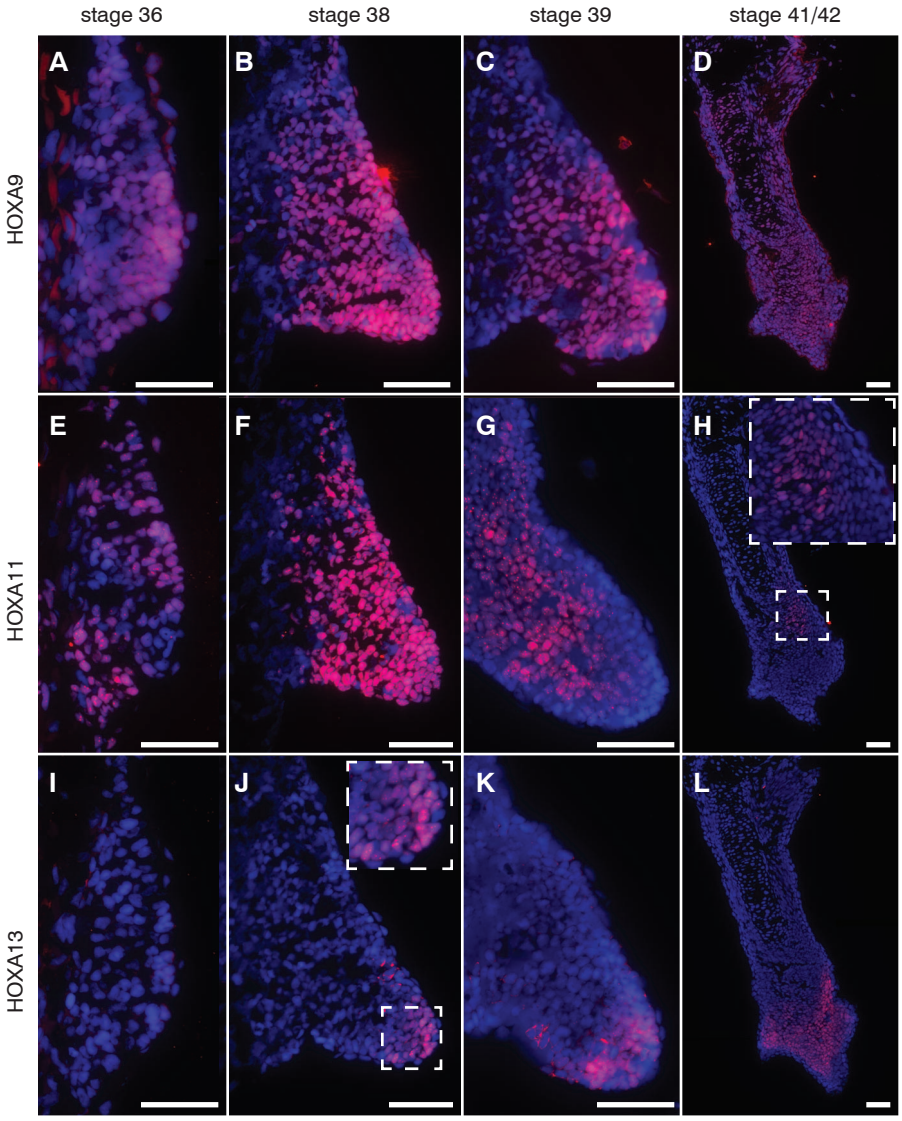

Fig. 1. Sequential expression of HOXA9, HOXA11, and HOXA13 during axolotl limb development. At stage 36, HOXA9 is expressed in the nascent limb bud (**A**), onset of HOXA11 expression is evident (**E**), and HOXA13 is absent (**I**). At stage 38, HOXA9 is expressed throughout the limb bud (**B**), HOXA11 is expressed with a more distal expression boundary (**F**), and HOXA13 is expressed in distal cells (**J**). At stage 39, HOXA9 is expressed throughout the limb bud (**C**), HOXA11 is depleted from the distal limb bud (**G**), and HOXA13 is expressed in distal cells (**K**). At stages 41/42, HOXA9 is expressed throughout the limb (**D**), HOXA11 is expressed in a small zone distal to the differentiating humerus and proximal to the emerging hand (**H**), and HOXA13 is the distal region differentiating hand (**L**). Hoechst nuclear signal is in blue. Anterior is at top; posterior, down; and distal, right. Scale bars indicate 100 μm.

progenitor cells are specified in a proximal-to-distal sequence, although some intercalation models have been proposed (*24*–*27*).

Important work localizing *HoxA9* and *A13* transcripts in the regenerating *Ambystoma mexicanum* (axolotl) limb described coexpression of *HoxA13* with *HoxA9* at the earliest time points of regeneration, with emergence of a nested pattern later. Such coexpression suggested an unusual violation of colinearity and was consistent with the possibility of intercalation (*28*). The whole-mount analysis did not, however, yield cellular resolution, so the source of the signal remained unclear. The limb tissue 1 to 2 days postamputation (dpa) is a watery infiltrate of inflammation and clotting-associated material. Immune cells rather than prospective blastema cells could, for example, have been a source of signal (*29*). Therefore, despite a historically strong interest in intercalation, definitive molecular or functional evidence for this mechanism was lacking. We reexplored this issue at higher molecular and cellular resolution.

We first examined the progression of HOXA9, A11, and A13 protein expression in axolotl limb development and confirmed spatial and temporal colinear expression (Fig. 1 and fig. S2) (*21*–*23*, *28*). We next examined the sequence of HOXA protein expression in the regenerating upper limb blastema, including early time points. Because a morphologically defined blastema is not evident at 1 day, we examined limbs in which the relevant blastema precursors (connective tissue cells) expressed enhanced GFP (eGFP). We did not observe HOXA9, A11, or A13 signal in blastema cells at 1 day (Fig. 2, A and B, and fig. S3). In particular, none of the HOXA13 immunofluorescence signal observed at 1 day colocalized with GFP^+. HOXA13 was also absent at 4 dpa (fig. S4). By early-bud stage (6 dpa), HOXA9 and HOXA11 expression was evident throughout the blastema, but HOXA13 expression was still absent (Fig. 2, C, E, and G). By medium- and late-bud stages (8 and 12 dpa), a complete nested pattern was observed, with HOXA13 expressed strongly at the distal tip (Fig. 2, D, F, and H, and fig. S4, F to I). The late onset of *HoxA13* expression was corroborated by section in situ hybridization (fig. S5). Therefore, during regeneration posterior HOXA expression occurs colinearly, as in limb development, suggesting that regenerating limb segments are specified in a proximal-to-distal order and not by intercalation.

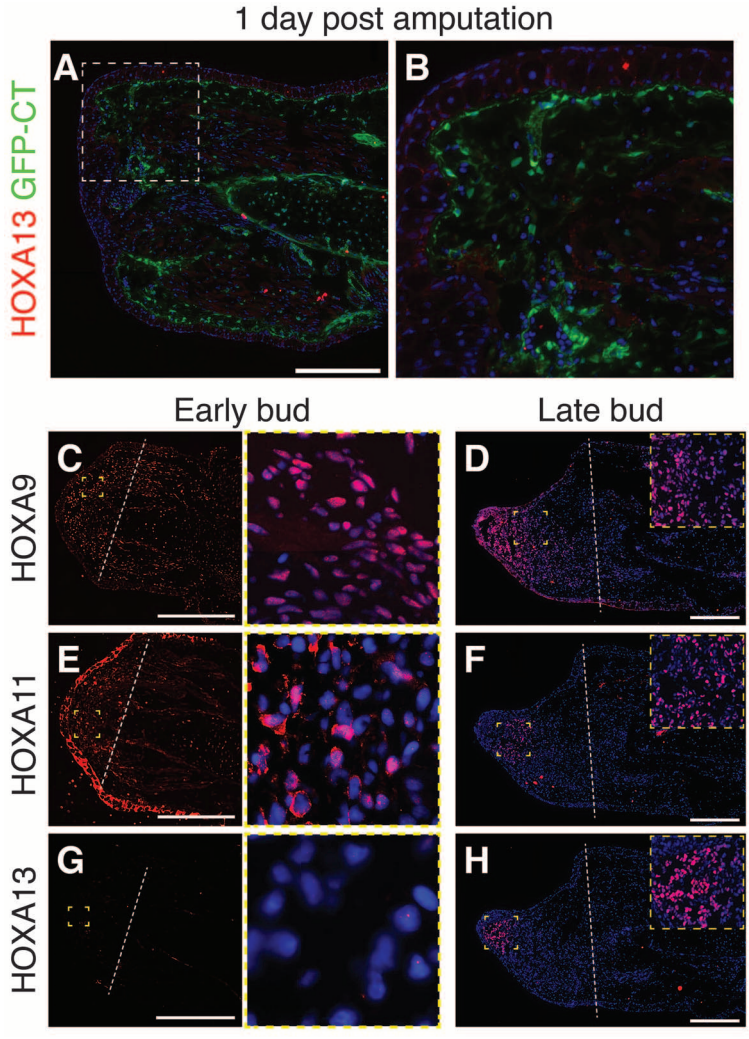

Fig. 2. Sequential expression of HOXA9, A11, and A13 protein during axolotl limb regeneration. Serial longitudinal sections of regenerating upper arm blastemas at 1 dpa, early bud (6 dpa), and late bud (12 dpa) immunostained for AxHOXA9, AxHOXA11, or AxHOXA13. (**A**) At 1 dpa, GFP-expressing blastema cell precursors from connective tissue (green) do not express HOXA13 (red). Image was taken at same exposure as in (H). (**B**) Zoom of area outlined in (A). Early bud blastema (6 dpa) expresses robust HOXA9 (**C**) and nascent HOXA11 (**E**) but does not express HOXA13 (**G**). Images at right show nuclei at higher zoom in positive zones. Late-bud blastema (12 dpa) expresses robust HOXA9 (**D**) and HOXA11 (**F**) and HOXA13 (**H**). HOXA9 is positive broadly in the blastema, HOXA11 in a medial band, and HOXA13 at the distal tip. Insets show positive nuclei at higher zoom. Dashed line, plane of amputation; distal, left; proximal, right. Scale bars, 500 μm.

To confirm the association of HOXA13 expression with hand identity, we examined the onset of HOXA13 expression in hand amputations where we first detected signal already at 4 dpa and strongly by 6 dpa—well before onset of HOXA13 expression in the upper arm blastema (fig. S6). Systemic administration of retinoic acid (RA) is known to convert a hand blastema into an upper arm blastema (*30*–*33*). RA-treated hand blastemas at 4 and 6 dpa showed no detectable HOXA13 expression, confirming the sensitivity of HOXA13 immunostaining in detection of a hand determination state.

To functionally assess the order of blastema cell specification, we used transplantation to assay whether early upper-arm blastema cells have already acquired hand identity, as would be predicted by the intercalation model (Fig. 3 and fig. S7). Donor connective tissue–derived cells constitutively expressed eGFP from a genomically inserted transgene (*12*, *13*). Control, medium-bud (8-day) hand blastema cells contributed only to hand structures when transplanted into a 6-day upper-arm blastema (Fig. 3, A, B, I, and J) (*12*, *33*). Transplantation of distal tip cells from medium-bud upper-arm blastemas ($HOXA13^+$) yielded distributions very similar to those of the hand blastema transplantations showing commitment of distal ($HOXA13^+$) cells to hand by medium-bud stage (Fig. 3, C, D, I, and J). Donor cells from the proximal base of the 8-day upper-arm blastema distributed in both the lower arm and the hand, corresponding to $HOXA9^+HOXA13^-$ upper-arm progenitor cell potential (Fig. 3, E, F, I, and J). Last, transplantation of the distal tip of early (4-day) blastema cells (pre-HOXA13) yielded cells in lower arm and hand (Fig. 3, G to J) corresponding to upper arm properties rather than hand-only identity. Taken together, these results indicate that blastema cells are specified in a proximal-to-distal sequence during regeneration rather than through intercalation.

In summary, HOXA protein data and functional assays indicate that, during axolotl limb regeneration, cell identities are specified in a proximal-to-distal order rather than by intercalation, indicating that the patterning mechanisms used in development and regeneration are similar. Although intercalation may not be the patterning mechanism underlying normal limb regeneration, intercalation

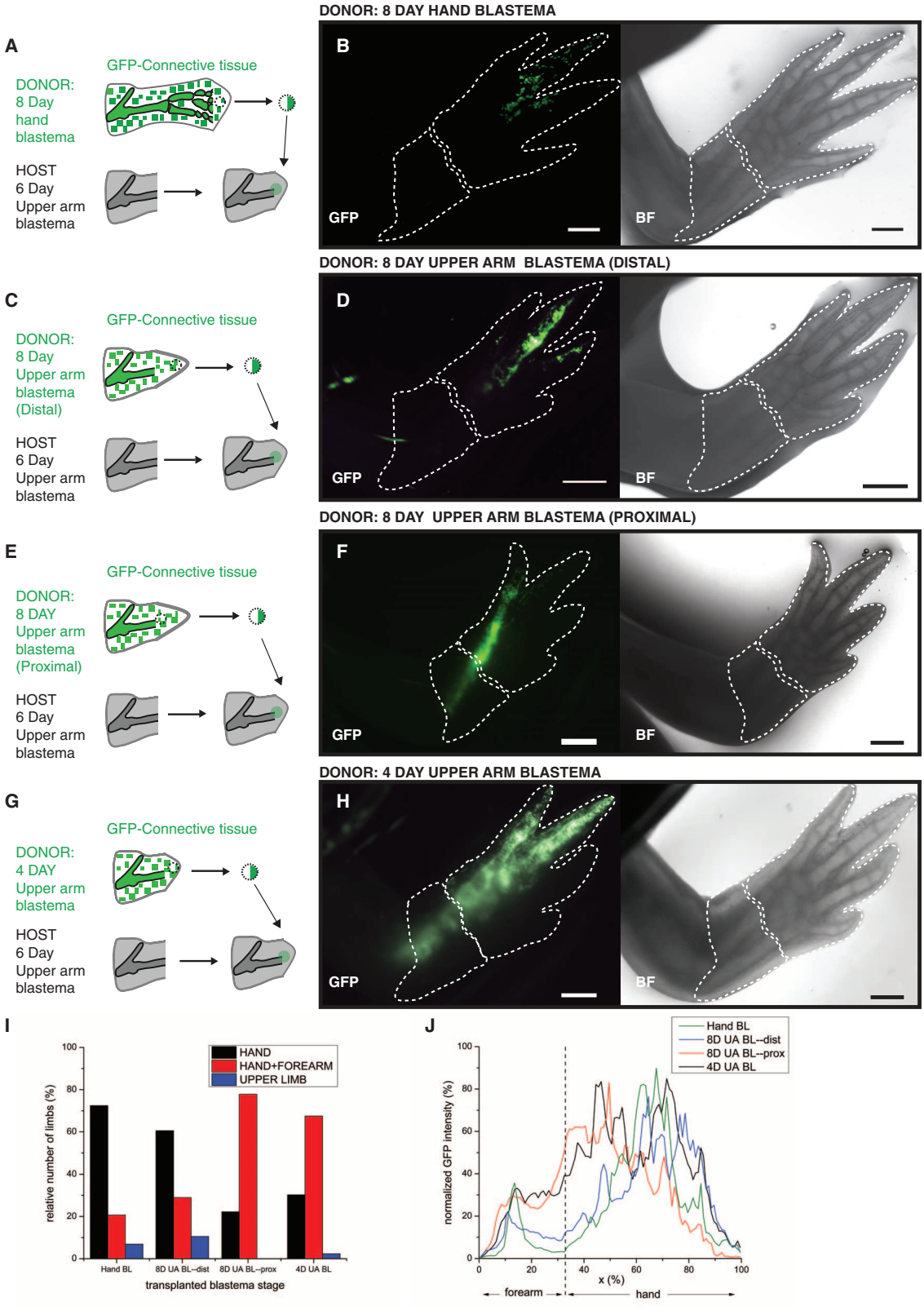

Fig. 3. Early blastema cells are not committed to a hand fate. Commitment to hand identity correlates with late onset of HOXA13 expression. Grafts of GFP-expressing connective tissue–derived blastema cells from different-stage blastemas were made into 6-day upper-arm blastema hosts to assay commitment to hand identity. (**A**) Schema of 8-day hand blastema (HOXA13^{+}) transplanted into 6-day upper-arm blastema. (N = 29) (**B**) Representative experimental result of (A): GFP^{+} cells were found in hand. (**C**) Schema of a distal region of an 8-day upper arm blastema (HOXA13^{+}) transplanted into 6-day blastema of a white host (N = 38). (**D**) Representative experimental result of (C): GFP^{+} cells were detected in the hand. (**E**) Schema of a proximal region of an 8-day upper-arm blastema (HOXA13^{-}) transplanted into 6-day blastema of a white host (N = 27). (**F**) Representative experimental result of (E): GFP^{+} cells were found all along the regenerated proximal/distal (P/D) axis. (**G**) Schema of an early 4-day upper-arm blastema (pre-HOXA13) transplanted into a 6-day blastema host (N = 43). (**H**) Representative experimental result of (G). Upon regeneration, GFP^{+} cells were detected all along the P/D axis in the host. Dashed lines in (B), (D), (F), and (H) indicate the outline of the lower arm and hand. Scale bar, 1 mm. (**I**) The fraction of limbs showing GFP^{+} cells in hand only, hand and forearm, or in the upper arm for each transplantation category. Samples showing upper arm only (blue bar) represent samples where transplant was stuck at amputation plane. (**J**) Averages of normalized GFP fluorescence along the proximodistal axis for limbs in the different transplantation categories. The normalized lengths of the forearm and the hand calculated for all the limbs studied are indicated. *x* represents the percent distance between the base of the forearm and the tip of the hand. Standard deviations of the data are in fig. S7. D, day; UA, upper arm; BL, blastema.

and other cell-cell recognition events likely play a role in certain grafting situations and possibly in fine-tuning patterning via segment-specific adhesive properties (*34*–*36*).

References and Notes

1. V. French, P. J. Bryant, S. V. Bryant, *Science* **193**, 969–981 (1976).
2. M. Maden, *J. Theor. Biol.* **69**, 735–753 (1977).
3. S. V. Bryant, V. French, P. J. Bryant, *Science* **212**, 993–1002 (1981).
4. J. E. Mittenthal, *Dev. Biol.* **88**, 15–26 (1981).
5. H. Meinhardt, *J. Embryol. Exp. Morphol.* **76**, 139–146 (1983).
6. H. Meinhardt, *J. Embryol. Exp. Morphol.* **76**, 115–137 (1983).
7. H. Bohn, *Roux's Arch.* **165**, 303–341 (1970).
8. D. L. Stocum, *Dev. Biol.* **45**, 112–136 (1975).

9. L. E. Iten, S. V. Bryant, *Dev. Biol.* **44**, 119–147 (1975).
10. M. J. Pescitelli Jr., D. L. Stocum, *Dev. Biol.* **79**, 255–275 (1980).
11. E. G. Butler, H. F. Blum, *J. Natl. Cancer Inst.* **15**, 877–889 (1955).
12. M. Kragl *et al.*, *Nature* **460**, 60–65 (2009).
13. E. Nacu *et al.*, *Development* **140**, 513–518 (2013).
14. J. Faber, *Arch. Biol. (Liege)* **71**, 1–72 (1960).
15. K. Echeverri, E. M. Tanaka, *Dev. Biol.* **279**, 391–401 (2005).
16. A. P. Davis, D. P. Witte, H. M. Hsieh-Li, S. S. Potter, M. R. Capecchi, *Nature* **375**, 791–795 (1995).
17. Y. Yokouchi *et al.*, *Genes Dev.* **9**, 2509–2522 (1995).
18. C. Fromental-Ramain *et al.*, *Development* **122**, 461–472 (1996).
19. C. Fromental-Ramain *et al.*, *Development* **122**, 2997–3011 (1996).
20. J. Zakany, D. Duboule, *Curr. Opin. Genet. Dev.* **17**, 359–366 (2007).
21. Y. Yokouchi, H. Sasaki, A. Kuroiwa, *Nature* **353**, 443–445 (1991).
22. H. Haack, P. Gruss, *Dev. Biol.* **157**, 410–422 (1993).
23. C. E. Nelson *et al.*, *Development* **122**, 1449–1466 (1996).
24. M. Towers, L. Wolpert, C. Tickle, *Curr. Opin. Cell Biol.* **24**, 181–187 (2012).
25. A. Roselló-Díez, M. Torres, *Dev. Dyn.* **240**, 1203–1211 (2011).
26. C. Tabin, L. Wolpert, *Genes Dev.* **21**, 1433–1442 (2007).
27. F. V. Mariani, C. P. Ahn, G. R. Martin, *Nature* **453**, 401–405 (2008).
28. D. M. Gardiner, B. Blumberg, Y. Komine, S. V. Bryant, *Development* **121**, 1731–1741 (1995).
29. H. J. Lawrence, G. Sauvageau, R. K. Humphries, C. Largman, *Stem Cells* **14**, 281–291 (1996).
30. S. Saxena, I. A. Niazi, *Indian J. Exp. Biol.* **15**, 435–439 (1977).
31. M. Maden, *Nature* **295**, 672–675 (1982).
32. N. Mercader, E. M. Tanaka, M. Torres, *Development* **132**, 4131–4142 (2005).
33. K. Crawford, D. L. Stocum, *Development* **104**, 703–712 (1988).
34. N. Wada, H. Tanaka, H. Ide, T. Nohno, *Dev. Biol.* **264**, 550–563 (2003).
35. S. M. da Silva, P. B. Gates, J. P. Brockes, *Dev. Cell* **3**, 547–555 (2002).
36. M. Barna, L. Niswander, *Dev. Cell* **12**, 931–941 (2007).

Acknowledgments: We are grateful to H. Andreas, J. Michling, B. Gruhl, S. Moegel, and M. Armstead for animal care; M. Tipsword and D. Drechsel for antibody production; D. Gardiner for unpublished *HoxA11* fragment; F. Martin for initial cloning attempts; and J. Rink, J. Currie, and A. Gavalas for comments. National Center for Biotechnology Information accession numbers of axolotl genes are as follows: *HoxA9*, JX975067; *HoxA11*, JX975068; *HoxA13*, JX975069. Grant support came from DFG-SFB655: From Cells to Tissues (DFG TA274/2), DFG TA274/5, central funds of the Max Planck Institute for Cell Biology and Genetics and the Center for Regenerative Therapies, and Human Frontiers Science Program (E.M.T.). A.T. and E.M.T. designed, conceived experiments, and analyzed data. K.R. and A.T. performed experimental work and analyzed data. O.C. developed and performed image analysis. K.R., A.T., and E.M.T. prepared the manuscript. The authors claim no competing interests.

Supplementary Materials

www.sciencemag.org/content/342/6164/1375/suppl/DC1
Materials and Methods
Figs. S1 to S7
References (*37*–*40*)

11 June 2013; accepted 1 November 2013
10.1126/science.1241796

EMRE Is an Essential Component of the Mitochondrial Calcium Uniporter Complex

Yasemin Sancak,[1,2] Andrew L. Markhard,[1] Toshimori Kitami,[1,2]* Erika Kovács-Bogdán,[1] Kimberli J. Kamer,[1] Namrata D. Udeshi,[2] Steven A. Carr,[2] Dipayan Chaudhuri,[3,4] David E. Clapham,[3] Andrew A. Li,[1] Sarah E. Calvo,[1,2] Olga Goldberger,[1] Vamsi K. Mootha[1,2]†

The mitochondrial uniporter is a highly selective calcium channel in the organelle's inner membrane. Its molecular components include the EF-hand–containing calcium-binding proteins mitochondrial calcium uptake 1 (MICU1) and MICU2 and the pore-forming subunit mitochondrial calcium uniporter (MCU). We sought to achieve a full molecular characterization of the uniporter holocomplex (uniplex). Quantitative mass spectrometry of affinity-purified uniplex recovered MICU1 and MICU2, MCU and its paralog MCUb, and essential MCU regulator (EMRE), a previously uncharacterized protein. EMRE is a 10-kilodalton, metazoan-specific protein with a single transmembrane domain. In its absence, uniporter channel activity was lost despite intact MCU expression and oligomerization. EMRE was required for the interaction of MCU with MICU1 and MICU2. Hence, EMRE is essential for in vivo uniporter current and additionally bridges the calcium-sensing role of MICU1 and MICU2 with the calcium-conducting role of MCU.

The mitochondrial calcium uniporter is a highly selective channel that moves calcium ions across the mitochondrial inner membrane (*1*). Although its physiology has been studied for decades, a complete description of its molecular composition has remained elusive. Recently, integrative genomics methods enabled the discovery of the uniporter pore, mitochondrial calcium uniporter (MCU), and its regulatory subunits, mitochondrial calcium uptake 1 and 2 (MICU1 and 2) (*2*–*5*). MCU is an integral membrane protein that is essential for the electrophysiologically defined uniporter current (*6*); it has two transmembrane domains and orients both its N and C termini into the matrix (*3*, *7*). MICU1 contains EF-hand calcium binding domains and is found in the mitochondrial intermembrane space (IMS), where it serves as a calcium-sensing gatekeeper, keeping the channel closed when calcium levels are low and allowing the channel to open in response to transient rises (*2*, *5*, *8*, *9*). Its paralog and binding partner, MICU2, has not been extensively characterized (*5*). Other proteins, including leucine-zipper EF-hand containing transmembrane protein 1 (LETM1), mitochondrial calcium uniporter regulator 1 (MCUR1), mitochondrial sodium calcium exchanger (NCLX), transient receptor potential 3 (TRPC3), and uncoupling protein 2 and 3 (UCP2 and 3) are also crucial for mitochondrial calcium physiology, but their physical relation to the uniplex are unclear (*10*–*14*).

[1]Department of Molecular Biology, Massachusetts General Hospital, Department of Systems Biology, Harvard Medical School, Boston, MA, USA. [2]Broad Institute of Massachusetts Institute of Technology and Harvard, Cambridge, MA, USA. [3]Howard Hughes Medical Institute, Department of Cardiology, Children's Hospital and Department of Neurobiology, Harvard Medical School, Boston, MA, USA. [4]Cardiovascular Research Center, Massachusetts General Hospital, Boston, MA, USA.

*Present address: RCAI, RIKEN Center for Integrative Medical Sciences, Yokohama, Japan.
†Corresponding author. E-mail: vamsi@hms.harvard.edu

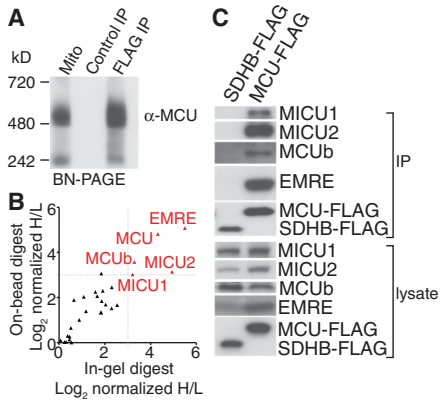

Fig. 1. Affinity purification and proteomic analysis of the uniplex. (A) MCU-FLAG or control SDHB-FLAG was stably expressed in HEK-293T cells. Proteins from digitonin-permeabilized mitochondria from MCU-FLAG–expressing cells and FLAG immunoprecipitations from SDHB-FLAG– and MCU-FLAG–expressing cells were subjected to blue native polyacrylamide gel electrophoresis (BN-PAGE) and immunoblotted with MCU antibody. **(B)** Identification of proteins that interact with MCU-FLAG. MCU-FLAG–expressing cells were grown in the presence of heavy amino acids; control HEK-293T cells were grown in the presence of light amino acids. FLAG immunoprecipitates from both samples were mixed and analyzed by mass spectrometry. The ratios of heavy and light proteins annotated with mitochondrial localization from two replicates are shown. Proteins that show more than eight-fold enrichment in heavy samples are shown in red. **(C)** Interaction of MCUb, MICU1, MICU2, and EMRE with MCU. MCU-FLAG or control SDHB-FLAG was immunoprecipitated from HEK-293T cells. Immunoprecipitates and cell lysates were analyzed by immunoblotting for the indicated proteins.